Nanotoxicology

ISSN: 1743-5390 (Print) 1743-5404 (Online) Journal homepage: https://www.tandfonline.com/loi/inan20

Mitoxantrone-loaded superparamagnetic iron oxide nanoparticles as drug carriers for cancer therapy: Uptake and toxicity in primary human tubular epithelial cells

Iwona Cicha, Laura Scheffler, Astrid Ebenau, Stefan Lyer, Christoph Alexiou & Margarete Goppelt-Struebe

To cite this article: Iwona Cicha, Laura Scheffler, Astrid Ebenau, Stefan Lyer, Christoph Alexiou & Margarete Goppelt-Struebe (2016) Mitoxantrone-loaded superparamagnetic iron oxide nanoparticles as drug carriers for cancer therapy: Uptake and toxicity in primary human tubular epithelial cells, Nanotoxicology, 10:5, 557-566, DOI: 10.3109/17435390.2015.1095364

To link to this article: https://doi.org/10.3109/17435390.2015.1095364

http://informahealthcare.com/nan
ISSN: 1743-5390 (print), 1743-5404 (electronic)

Nanotoxicology

Nanotoxicology, 2015; 10(5): 557–566
© 2015 Taylor & Francis. DOI: 10.3109/17435390.2015.1095364

Taylor & Francis
Taylor & Francis Group

ORIGINAL ARTICLE

Mitoxantrone-loaded superparamagnetic iron oxide nanoparticles as drug carriers for cancer therapy: Uptake and toxicity in primary human tubular epithelial cells

Iwona Cicha[1], Laura Scheffler[2], Astrid Ebenau[2], Stefan Lyer[1], Christoph Alexiou[1], and Margarete Goppelt-Struebe[2]

[1]*Section of Experimental Oncology and Nanomedicine (SEON), ENT Department, Else Kröner-Fresenius-Stiftungsprofessur, University Hospital Erlangen, Germany and* [2]*Department of Nephrology and Hypertension, Friedrich-Alexander Universität Erlangen-Nürnberg, Germany*

Abstract

Superparamagnetic iron oxide nanoparticles (SPIONs) are in use for many clinical diagnostic and experimental therapeutic applications, for example, for targeted drug delivery. To analyze the cellular responses to mitoxantrone-carrying SPIONs (SPION-MTO), and to the drug released from SPIONs, we used an *in vitro* system that allows comparison of primary human cells with different endocytotic capacities, namely, epithelial cells from proximal and distal parts of the nephron. SPIONs were selectively and rapidly internalized by proximal tubular cells with high endocytotic potential, but not by distal tubular cells. Uptake did not affect cell viability or morphology. In both cell types, free MTO (10–100 nM) induced double-strand DNA breaks and senescence, cell hypertrophy and reduced cell proliferation. However, cadherin-mediated cell–cell adhesion, cytoskeletal structures or polarity of the cells were not affected. Interestingly, a comparable response was also observed upon treatment with SPION-MTO and was independent of uptake of the particles. The effect of SPION-MTO on cells which did not internalize particles was primarily related to the release of MTO from drug-coated particles upon incubation in serum-containing cell growth medium. In conclusion, we show that whereas the uptake of SPIONs does not affect cellular functions or viability, the toxicity of drug-loaded SPIONs depends essentially on the type of drug bound to nanoparticles. Due to the relatively low systemic toxicity of MTO, the effects of MTO-SPIONs on human tubular cells were moderate, but they may become clinically relevant when more nephrotoxic drugs are bound to SPIONs.

Keywords

Drug delivery, magnetic nanoparticles, nephrotoxicity, senescence, topoisomerase II

History

Received 4 May 2015
Revised 12 August 2015
Accepted 10 September 2015
Published online 13 October 2015

Introduction

Superparamagnetic iron oxide nanoparticles (SPIONs) are in use for many diagnostic applications, such as magnetic resonance imaging (MRI) of lymph nodes, liver, intestines and the cardiovascular system. Additionally, their use for therapeutic applications (drug delivery, and hyperthermia) continues to increase (Amstad et al., 2011; Gupta & Gupta, 2005; Laurent et al., 2014). SPIONs consist of an iron oxide core, often coated with organic materials, such as fatty acids, polysaccharides or polymers (Wahajuddin & Arora, 2012). Coating stabilizes the nanoparticles and allows stable the conjugation of specific affinity ligands, radiotracers or fluorochromes, offering the possibility of multimodal imaging of intracellular targets. Moreover, the magnetic properties of SPIONs allow the remote control of their accumulation by means of an external magnetic field. These physical properties together with their low cytotoxicity in mammalian cells and organisms (Jeng & Swanson, 2006) predict a broad usage of SPIONs in biomedicine.

Correspondence: Margarete Goppelt-Struebe, PhD, Friedrich-Alexander-Universität Erlangen-Nürnberg, Department of Nephrology and Hypertension,, Loschgestrasse 8, D-91054 Erlangen, Germany. Tel: +49-9131-8539201. Fax: +49-9131-8539202. E-mail: margarete.goppelt-struebe@uk-erlangen.de

Conjugation of SPIONs with drugs, in combination with an external magnetic field to target the nanoparticles (so-called magnetic drug targeting, (MDT)), has recently emerged as a promising strategy to overcome the problems associated with systemic chemotherapeutic approaches in cancer patients. This form of drug delivery is expected to concentrate the therapeutic agent at the site of action by accumulating drug-loaded SPIONs in the target region. Indeed, our previous studies in a rabbit model of VX-2 carcinoma implanted subcutaneously into the left hind limb showed that upon a single intraarterial application of mitoxantrone (MTO)-carrying SPIONs, increased drug payloads in the target tissue are achieved under a strong external magnetic field (Janko et al., 2013; Lyer et al., 2010; Tietze et al., 2013). This increases the therapeutic efficacy of the drug, at the same time reducing its systemic dose and toxicity.

SPIONs have been reported to have favorable safety profiles (Bernd et al., 2009), but delayed toxicity effects due to an increased inflammation and oxidative stress cannot be excluded (Winer et al., 2012). The cellular effects of different SPIONs may furthermore differ depending on their size, charge, and coating (Albanese et al., 2012).

Although the concept of MDT encompasses a localized delivery of drug-loaded nanoparticles to the diseased organs or tissues while minimizing the systemic side effects, even under intraarterial administration, low concentrations of drug-loaded

SPIONS will escape the magnetic field and accumulate in other organs (Tietze et al., 2013). Additionally, as the SPIONs evade renal clearance due to their size, an increased circulation half-life of the transported drugs can occur. Biological effects of drug-loaded SPION within the organs will thus be determined both by the exposure to drug-loaded SPIONs, as well as by the amount of free drug released from the SPIONs.

To analyze the different aspects of cellular responses to drug-carrying SPIONs, and to the drug released from SPIONs, we set up an *in vitro* system that allows comparison of primary human cells with different endocytotic capacities. This model is based on epithelial cells lining the kidney nephron, which differ largely in their capacity to take up material. *In vivo*, proximal tubular cells are responsible for reabsorption of proteins from the tubular lumen to prevent proteinuria (Kriz & LeHir, 2005). Additionally, these cells rapidly endo/phagocytose environmental toxins and bacteria, which renders them more susceptible to injuries (Nagai & Takano, 2014; Saito et al., 2010). In contrast, distal tubular cells responsible for regulating ion transport are characterized by a very low internalization of larger molecules or particles. Proximal tubular cells are the only epithelial cells in the human adult organism which express *N*-cadherin instead of *E*-cadherin as major cell-cell adhesion protein, which allows the differentiation of SPION uptake by isolated cells of proximal and distal origin by immunocytochemistry (Kroening et al., 2010). In this study, we utilized a drug-carrying nanosystem comprising an iron oxide core coated with lauric acid and loaded with MTO, which was effectively used for MDT application in a rabbit model (Tietze et al., 2013; Zaloga et al., 2014). MTO is a well-characterized chemotherapeutic drug, which exerts its cytostatic effects primarily via inhibition of DNA topoisomerases II, the enzymes that generate transient double strand DNA breaks and are essential for DNA replication, recombination and separation of daughter chromosomes (McClendon & Osheroff, 2007). Cellular effects of nanoparticle-bound MTO and MTO released from SPIONs at low nanoparticle concentrations were investigated in primary cultures of human tubular epithelial cells.

Methods

Materials

X-gal (5-bromo-4-chloro-3-indolyl-β-*D*-galactopyranoside), lauric acid, iron (III) chloride hexahydrate, potassium ferrocyanide ($K_4[Fe(CN)_6]$), potassium ferricyanide ($K_3[Fe(CN)_6]$, and DAPI (4′,6-diamidino-2-phenylindole) were obtained from Sigma Aldrich. Iron (II) chloride tetrahydrate was purchased from Merck, and mitoxantrone from Teva GmbH, Ulm, Germany.

Synthesis of superparamagnetic iron oxide nanoparticles (SPIONs)

SPIONs were synthesized using the alkaline precipitation method and functionalized with mitoxantrone (SPION-MTO) by self-assembling adsorptive binding (Tietze et al., 2013). Control lauric acid-coated nanoparticles without MTO are referred to as SPIONs further in the text. Details of the preparation and characterization of SPION and SPION-MTO are given in the online supplement.

Cell culture

Human primary tubular epithelial cells (hTEC) were isolated from renal cortical tissues collected from healthy parts of tumor-nephrectomies, as described previously (Zuehlke et al., 2012). Isolation of human cells was approved by the local ethics committee and written consent was obtained from all donors.

For experiments, hTEC were seeded in medium containing 2.5% FCS to facilitate cell attachment. After 24 h, medium was replaced with FCS-free epithelial cell selective medium (DMEM/Ham's F12 medium containing 2 mM L-glutamine, 100 U/ml penicillin, 100 µg/ml streptomycin, insulin-transferrin-selenium supplement, 10 ng/ml epidermal growth factor, 36 ng/ml hydrocortisone and 4 pg/ml triiodothyronine). Polarized cells were cultured on permeable transwell inserts (Millicell PCF, Millipore) as described previously (Zuehlke et al., 2012). In all experiments, hTEC at passages 1–3 were used. Cells of proximal and distal origin were separated by their differential adherence to cell culture plastic. Trypsinization for 3 min resulted in a culture enriched in proximal cells (about 50 to 60% *N*-cadherin-positive cells), while the remaining cells were over 90% *E*-cadherin-positive and thus represented cells of distal tubular origin. Cells obtained from 16 different donors were used in this study. Each graph represents experiments performed with cells obtained from at least two different donors.

Live cell imaging

Cells were seeded in 96-well plates (at 5000 cell per well) and were monitored every hour for 72 h using the live cell imaging system Incucyte FLR (Essen Bioscience, Ann Arbor). For the last 3 h, nuclei of the cells were labeled with Syto16 (0.25 µM, Molecular Probes, Life Technologies) to allow cell counting.

Prussian blue staining of SPIONs

After fixation with paraformaldehyde (3.5% in PBS), cells were incubated with 1% potassium ferrocyanide in 1% HCl for 30 min at room temperature. Immunocytochemical staining was performed after Prussian blue staining.

Immunocytochemistry

Cells were permeabilized by 0.5% Triton X-100 in phosphate-buffered saline (PBS) for 10 min, washed three times with PBS, and blocked in 1% BSA in PBS. The following antibodies were used for immunocytochemistry: anti-*E*-cadherin (#1416, Abcam), anti-*N*-cadherin (Sc7939, Santa Cruz), anti-phosphorylated (Ser 139) histone2AX (γH2AX, 2F3m, BioLegend), antitubulin (T0198, Sigma-Aldrich). PromoFluor 488- or 555-conjugated secondary antibodies were from PromoKine.

After mounting, slides were viewed using a Nikon Eclipse 80i fluorescent microscope and digital images recorded by Visitron Systems 7.4 Slider camera using Spot Advanced software (Diagnostic Instruments). Combined fluorescence and phase contrast images were obtained with a Keyence BZ9000 microscope (Keyence GmbH, Germany). Polarized cells were analyzed by epifluorescence microscopy including Apotome technique (Zeiss, Germany).

Quantification of γH2AX staining

hTEC were seeded on coverslips coated with collagen IV. Confluent cells were then incubated with MTO or SPION-MTO for 2 h and 4 h. After fixation with PFA, cells were treated with antibodies directed against γH2AX. Nuclei were stained with DAPI. Three areas of each coverslip were randomly chosen and photographs were taken under identical conditions. ImageJ software was used to determine the number of γH2AX-positive nuclei and to determine the total number of cells. The ratio γH2AX to cell number was used for comparison. In each experiment, the mean value of control cells was set to 1.

Determination of senescence

As a marker of senescence, β-galactosidase activity was detected at pH 6, as described by Dimri et al (Dimri et al., 1995) with X-gal as substrate. To determine cell numbers, hTEC were stained with DAPI. To quantify senescence-associated β-galactosidase

activity, three areas of each coverslip were randomly chosen and photos were taken under identical conditions. ImageJ software was used to determine X-gal positive areas and the total number of cells. The ratio of both was used for comparison. In each experiment, the mean value of control cells was set to 1.

Statistical analysis

To compare multiple conditions, statistical significance was calculated by one-way analysis of variance (ANOVA) with Tukey's multiple comparison test using GraphPad software (La Jolla, CA). A value of $p < 0.05$ was considered to indicate significant differences.

Results

Uptake of SPIONs by proximal tubular epithelial cells

Cells were incubated with different concentrations of SPIONs and uptake of particles was monitored by Prussian blue assay. It must be noted that experiments with hTECs are usually performed in medium without FCS to maintain the epithelial phenotype. However, dilution of SPIONs in this medium resulted in aggregation of the particles. Therefore, SPIONs were diluted in medium containing 2.5% FCS, resulting in a final FCS concentration of 1.25% FCS in all experiments. Incubation in this medium for up to 72 h did not change the phenotype of the epithelial cells, which retained their specific cell–cell adhesion molecules as shown in Figure 1.

Following incubation with control SPIONs, cells were stained by indirect immunofluorescence for *N*-cadherin as marker of human proximal tubular cells (Figure 1A, red) and *E*-cadherin for the cells of distal origin (Figure 1A, green) in order to distinguish between epithelial cells derived from different parts of the nephron. Within 2–4 h of incubation, SPIONs were rapidly taken up by the proximal cells, but not by distal epithelial cells. Prolonged culture of the cells for up to 72 h did not alter the distribution of SPIONs (Figure 1B). Epithelial cells formed confluent monolayers and viability of the cells was not affected as no change in cell numbers was observed after 72 h upon treatment with control SPIONs (Figure 1C).

Uptake of SPION-MTO by renal epithelial cells

Uptake of MTO-coated SPIONs (0.01 µg/ml MTO attached to SPIONs, corresponding to 0.02 µM MTO and 0.5 µg/ml Fe) was also observed preferentially in proximal tubular cells within the first 2–4 h (Figure 2A). However, this specificity was lost, when the cells were incubated with SPION-MTO for 72 h (Figure 2B). At this time point, uptake was no longer restricted to proximal cells, and Prussian blue-stained particles were also detected in *E*-cadherin positive cells of distal origin. However, loading of the cells with particles varied largely. The accumulation of SPION-MTO in a perinuclear area was primarily observed in proximal tubular cells (arrows in Figure 2B). As the cells were seeded as subconfluent cells and became confluent over the time course of 24 to 48 h, it was hypothesized that dividing distal cells might be more capable of taking up SPION-MTO than resting cells. To test

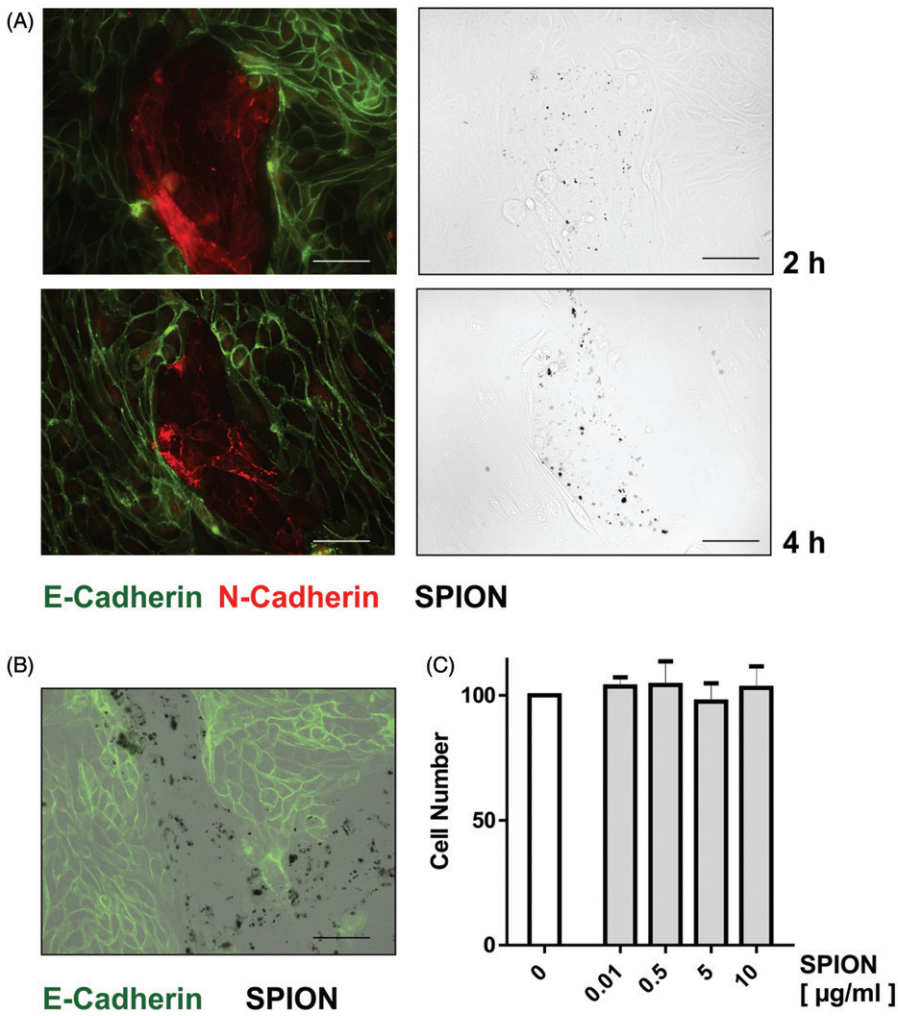

Figure 1. SPIONs are taken up by proximal tubular epithelial cells. (A) hTEC were incubated with SPIONs (5 µg/ml Fe) for 2 and 4 h. *E*- and *N*-cadherin were detected by indirect immunofluorescence (left panels) and SPION were visualized by Prussian blue staining. Scale bars: 60 µm. (B) hTEC were incubated with SPIONs (5 µg/ml Fe) for 72 h. *E*-cadherin was detected by indirect immunofluorescence, SPIONs were visualized by Prussian blue staining. Scale bar: 60 µm. (C) hTEC were incubated with different concentrations of SPIONs in triplicate for 72 h. Nuclei were stained with Syto16. Data are means ± SD of four different experiments, each with proximal and distal cell preparations.

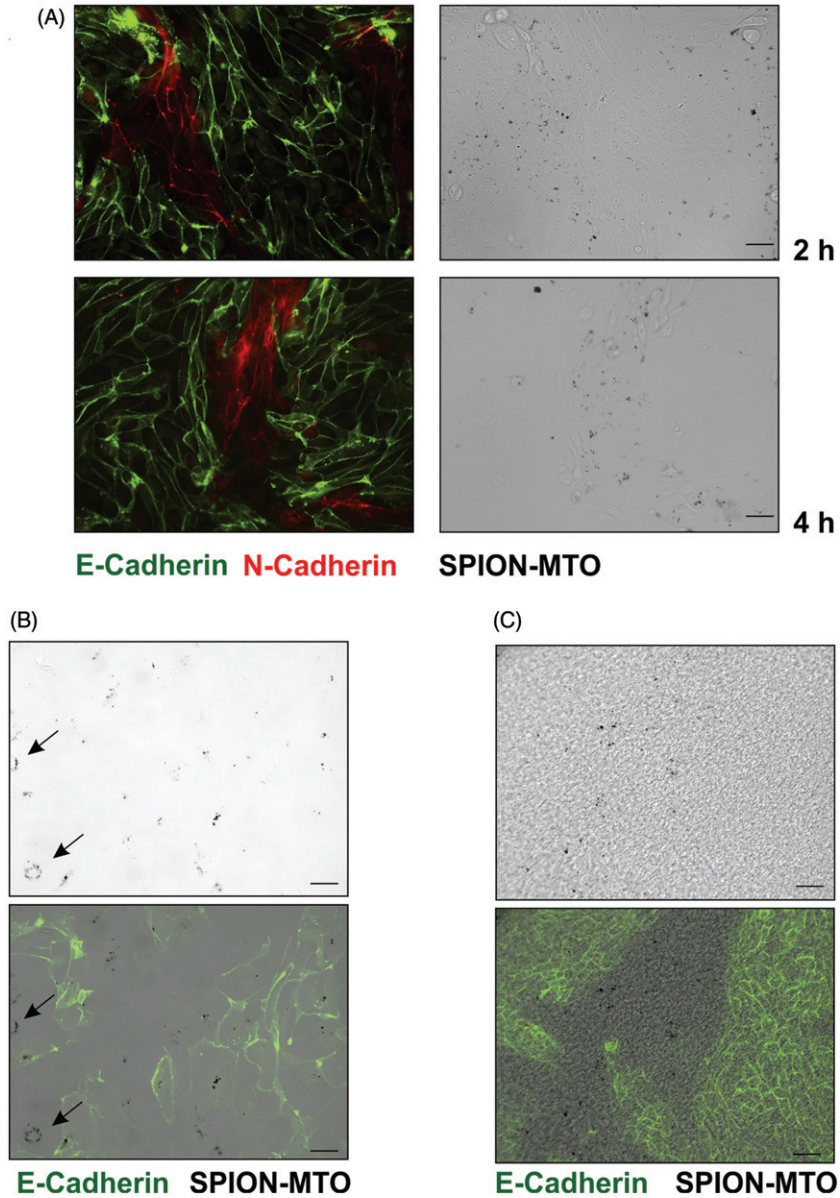

Figure 2. Uptake of SPION-MTO. (A) hTEC were incubated with SPION-MTO (0.1 μg/ml) for 2 and 4 h. *E*- and *N*-cadherin were detected by indirect immunofluorescence (left panels) and SPIONs were visualized by Prussian blue staining (right panels). Scale bars: 60 μm. (B) hTEC were incubated with SPION-MTO (0.01 μg/ml) for 72 h. Particles were visualized by Prussian blue staining (upper panel) and distal epithelial cells were stained with *E*-cadherin, (lower panel, green). Scale bars: 60 μm. (C) hTEC were polarized in transwell inserts and then treated with SPION-MTO (0.01 μg/ml) for 72 h. Staining was performed as in (B). Scale bars: 60 μm.

this hypothesis, we used polarized epithelial cells after 8 days of culture, which formed a dense monolayer and hardly proliferated. These cells were cultured on porous membranes visible as background in phase contrast images. In polarized cells, uptake of SPION-MTO was again restricted to proximal cells, even after 72 h (Figure 2C), supporting the hypothesis that cell division favored the uptake of SPION-MTO by distal tubular cells.

Comparison of SPION-treated cells (Figure 1B) and SPION-MTO-treated cells (Figure 2B), indicated hypertrophy and reduced cell numbers in the presence of SPION-MTO. Such cellular alterations may have contributed to the different uptake characteristics of the nanoparticles.

MTO interferes with epithelial cell proliferation

To assess cell proliferation, cell numbers of hTEC were determined after 72 h of culture with various concentrations of free MTO and SPION-MTO and compared to untreated cells or cells treated with control SPIONs (5 μg/ml Fe). Even at high concentrations of 5 μg/ml Fe, control SPIONs had no effect on cell proliferation. In contrast, both free MTO and SPION-MTO reduced cell numbers comparably and dose-dependently. A significant inhibition was observed at 1 ng/ml SPION-MTO, corresponding to ~2 nM MTO and 50 ng/ml Fe, whereas a saturating effect was observed at 5 ng/ml SPION-MTO (Figure 3B). Data obtained in cells incubated for 48 or 72 h were combined as there was no significant difference between those time points, indicating an early effect of MTO. Quantification of cell numbers showed comparable reduction of cell numbers by free MTO and SPION-MTO (Figure 3B). Furthermore, there was no significant difference between cell preparations of distal epithelial cells and cell preparations enriched in proximal tubular epithelial cells (Supplementary Figure 1). Concomitantly with the reduced cell numbers, an increase in the apparent size of the nuclei was observed (Figure 3C).

MTO does not impair cell–cell contacts or cell structures

It was previously reported that MTO may affect cells structures by inhibition of Rho GTPases (Bidaud-Meynard et al., 2013). To further characterize the effects of MTO on tubular epithelial cells, cells were treated for 48 h with 0.2 and 0.02 μg/ml MTO, concentrations, which completely blocked cell proliferation. Cell–cell borders were visualized by *E*-cadherin and integrity of the cytoskeleton by F-actin structures (Figure 4A). Even though MTO-treated cells were strongly enlarged, they did not lose

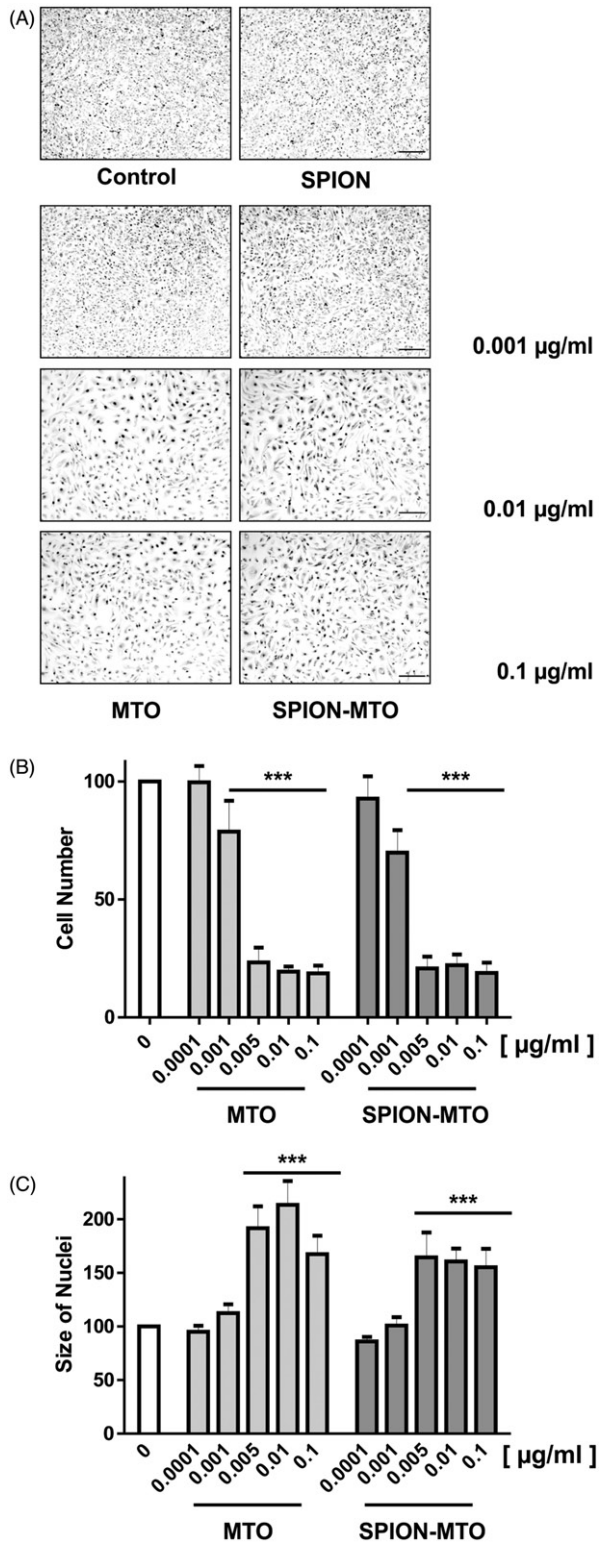

Figure 3. Inhibition of cell proliferation by MTO and SPION-MTO.
(A) hTEC were incubated with SPIONs (5 µg/ml Fe), MTO and SPION-MTO at the concentrations indicated. Nuclei were visualized by Syto16.
(B) Data are means ± SD of four different experiments with proximal and distal preparations. ***$p < 0.001$ compared to control cells, ANOVA with Tukey's multiple comparison test.
(C) Samples presented in B were used to determine the average size of the nuclei. ***$p < 0.001$ compared to control cells.

cell-cell contacts. The pattern of *F*-actin fibers was comparable in control cells and MTO-treated cells. When cultured on permeable filters, epithelial cells form highly organized polarized monolayers characterized by cilia oriented toward the apical side (Figure 4B, cilia stained by acetylated tubulin in red). Incubation with MTO (0.1 µg/ml) for up to 72 h did not affect the structural organization of polarized cells (Figure 4B). Similarly, microtubular structures were not affected by the treatment with MTO or SPION-MTO. As an example, incubation of hTECs for 72 h with SPION-MTO (0.01 µg/ml) and the corresponding concentration of SPIONs is shown in Figure 4C. As observed before, most but not all cells had taken up SPION-MTO particles and particle load was variable. However, structures of microtubules did not reflect the uptake of SPION-MTO. SPIONs were internalized only by cells of proximal origin, whereas those with structural features of distal cell were void of particles (Figure 4C, right panel). All cells showed regular microtubules. Live cell imaging revealed that in spite of their hypertrophy, the cells were moving without losing contact with neighboring cells (Supplementary videos 1 and 2).

MTO induces double-strand DNA breaks and senescence in tubular epithelial cells

MTO has been characterized as inhibitor of topoisomerase II, inducing double-strand DNA breaks. As a consequence, histone H2AX is phosphorylated at serine 139 (γH2AX) and accumulates at DNA strand breaks (McClendon & Osheroff, 2007). In our study, some weakly positive cells were detectable in control preparations (Figure 5A), in line with phosphorylation of H2AX in normal cells during cell cycle progression (Ichijima et al., 2005). However, the number of cells showing strongly positive phospho-H2AX foci was significantly increased upon treatment with MTO or SPION-MTO (Figure 5A, enlarged images Supplementary Figure 2). A tendency was already observed with 0.01 µg/ml MTO, which became highly significant with 0.1 µg/ml MTO or SPION-MTO as early as 4-h incubation time (Figure 5B). As shown in Figure 2, SPION-MTO were only taken up by cells of proximal origin during the short incubation period. Therefore, a correlation between γH2AX positive cells and cells containing particles was expected. However, as shown in Figure 5C, there was no correlation between particle content and histone phosphorylation (purple nuclei, overlay of blue DAPI-stained nuclei and red γH2AX fluorescence).

Development of cellular senescence upon MTO treatment has been observed in other cell types as a long-term consequence of topoisomerase II inhibition (Zhao et al., 2012). Therefore, senescence-associated β-galactosidase was determined as an indicator of senescent cells. Even under control conditions, some cells showed signs of senescence which was not unexpected after 72 h in culture (Figure 6, β-galactosidase activity in black, nuclei in green). Incubation with SPIONs did not significantly increase β-galactosidase activity (graph, Figure 6), whereas staining intensity was increased upon treatment with 0.001 µg/ml MTO or SPION-MTO and, even more dramatically, by 0.01 µg/ml MTO or SPION-MTO.

MTO is released from SPIONs in FCS-containing epithelial cell-specific medium

As a possible explanation for the effect of SPION-MTO on cells which had not taken up particles, we hypothesized that SPION-coated particles might release MTO either when in direct contact with the cells, or upon incubation in FCS-containing epithelial cell-specific cell medium. To test the latter hypothesis, SPION-MTO were diluted in medium containing 2.5% FCS and centrifuged at 12 000 rpm for 45 min. Subsequently, cells were treated with either the resulting supernatants or with SPION-MTO without centrifugation for 72 h. Cell numbers were reduced comparably by SPION-MTO and the supernatants, indicating that MTO is released from the nanoparticles into the FCS-containing medium (Figure 7A). To exclude specific effects of the

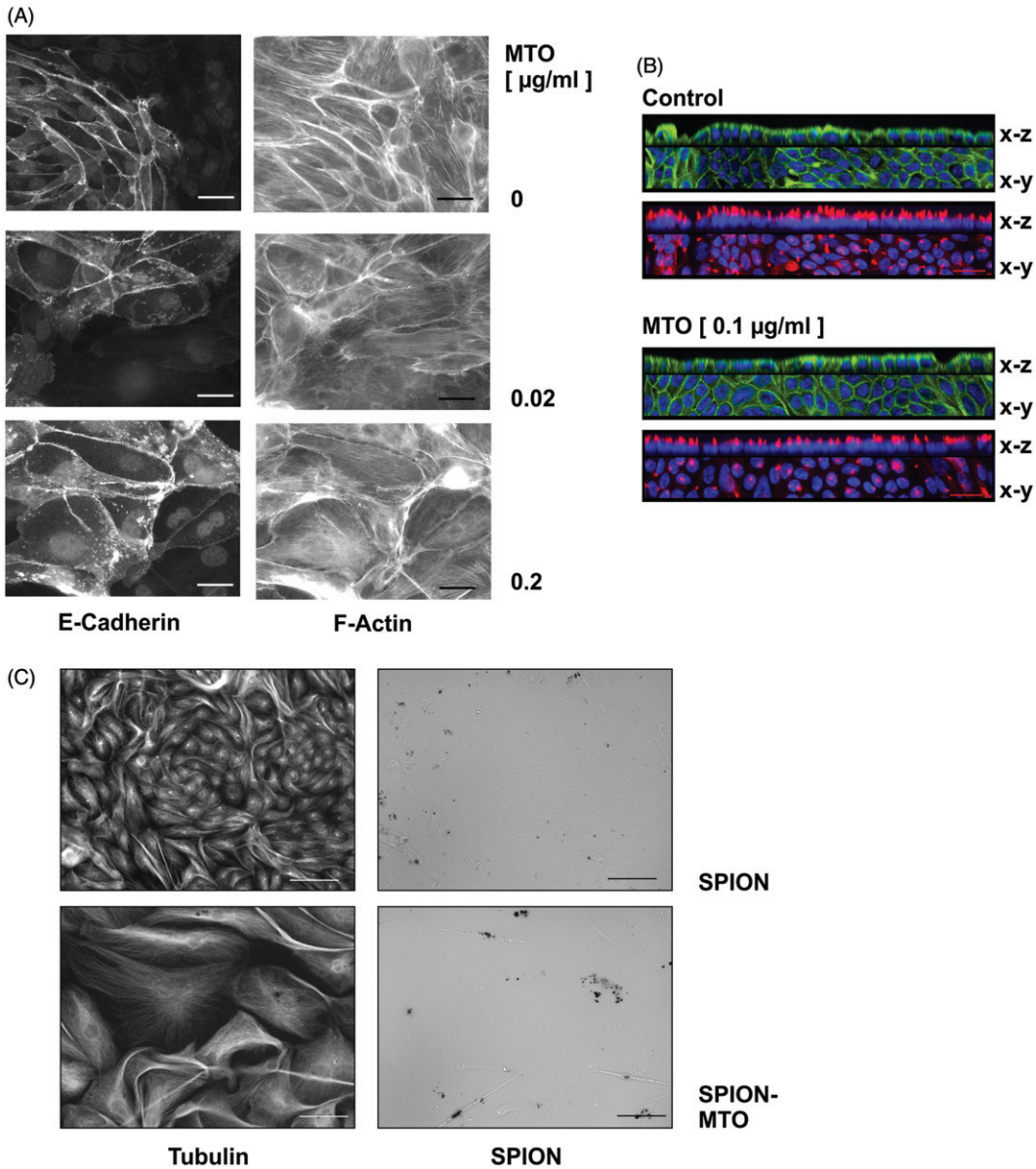

Figure 4. MTO does not alter cytoskeleton structures.
(A) hTEC were incubated with MTO for 48 h. Distal cells were visualized by E-cadherin staining. F-actin was detected by phalloidin. Scale bars: 30 µm.
(B) hTEC were polarized by cultivation in transwell inserts for 8 days. Cell were further incubated with MTO (0.1 µg/ml) for 72 h. *E*-cadherin (green) and acetylated tubulin as a marker of cilia (red) were detected by indirect immunofluorescence, nuclei were stained with DAPI. Images were generated using epifluorescence microscopy. Scale bar: 20 µm.
(C) hTEC were incubated with SPIONs or SPION-MTO (0.01 µg/ml) for 72 h. Tubulin was visualized by indirect immunofluorescence, SPIONs were detected by Prussian blue staining. Scale bar: 60 µm.

centrifugation process, cells were seeded on the membranes of trans-well chambers in subsequent experiments. Upon confluence, either MTO or SPION-MTO were added to the lower compartment. Although the size of the pores could not prevent SPION-MTO from interacting with the cells, sedimentation was expected to reduce contacts between nanoparticles and cells. Accordingly, particles were not detected in the cells (data not shown). However, cell numbers were significantly reduced by the presence of either free MTO or SPION-MTO, supporting the notion of MTO release from SPION-MTO in FCS-containing epithelial cell-specific medium (Figure 7B).

Discussion

Using the model system consisting of primary human tubular epithelial cells with different endocytotic capacities, we showed that SPIONs are taken up selectively by proximal, but not distal tubular cells. Proximal tubular cells reabsorb proteins and particles from the urine and are thus expected to be able to internalize SPIONs. In a healthy kidney, SPIONs with their hydrodynamic diameter of above 100 nm are too large to be filtered by the glomerulum but may be lost if the glomerular filtration barrier is impaired, as observed in many disease conditions (Kriz & LeHir, 2005). In line with data obtained with granulosa cells (Poettler et al., 2014) our study demonstrated that the uptake of SPIONs was well tolerated by proximal tubular cells and did not alter their viability, growth characteristics or morphology. Consequently, no differences were observed between cell which internalized SPIONs and untreated cells. In accordance with these results, a study by Soenen et al. (2010) provided evidence that the alterations of the actin cytoskeleton in neural progenitor cells and human blood outgrowth endothelial cells by iron oxide nanoparticles are concentration-dependent, and

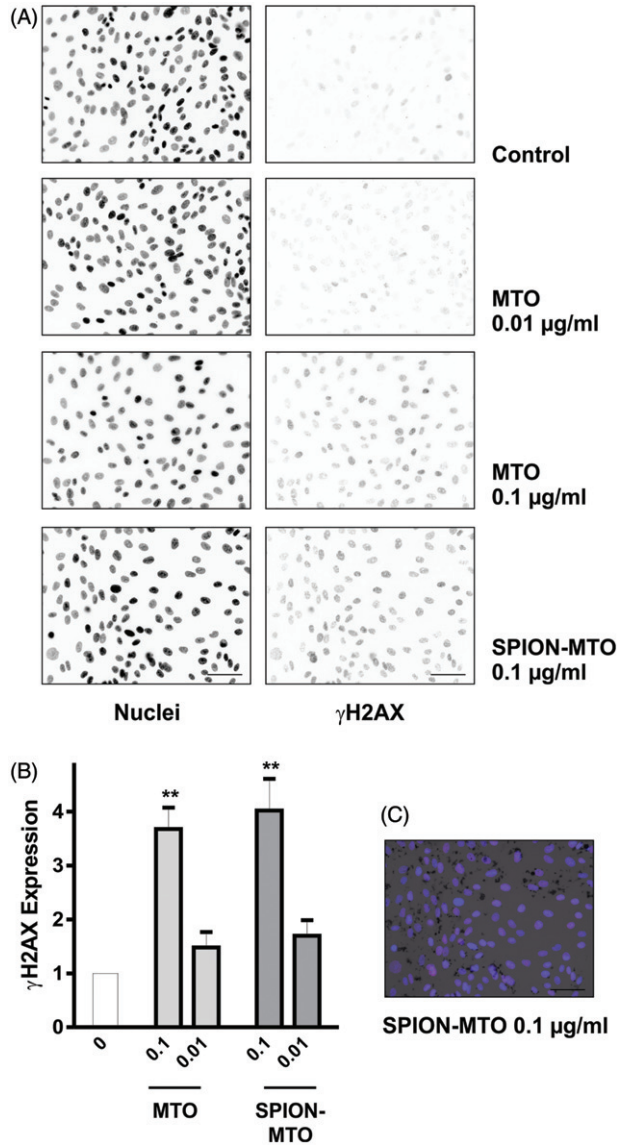

Figure 5. Increase in nuclear γH2AX by SPION-MTO is independent of particle uptake.
(A) hTEC were incubated with MTO or with SPION-MTO for 4 h. Cells were stained for γH2AX and nuclei were visualized by DAPI. Scale bar: 50 µm.
(B) Data are means ± SEM of three different preparations with three sections each. The mean number of γH2AX-positive cells in control incubations was set to 1 in each experiment ***$p < 0.001$, ANOVA with Tukey multiple comparison test, compared to control cells.
(C) Cells were treated as in (A). Nuclei (blue), γH2AX (red) and SPION (black) were merged. Scale bar: 60 µm.

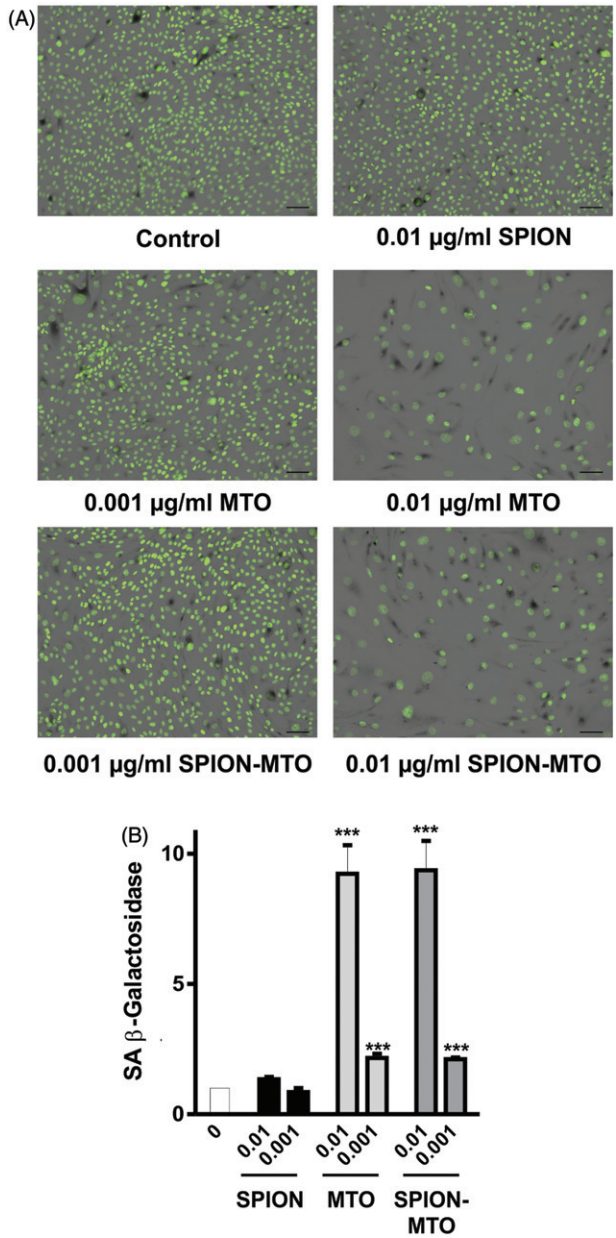

Figure 6. MTO and SPION-MTO induce senescence in hTEC.
hTEC were incubated with SPIONs, MTO or SPION-MTO (0.01 and 0.001 µg/ml) for 48 h. To assess senescence, the activity of senescence-associated (SA) β-galactosidase was detected by blue X-gal staining of the cells (converted to black in the figures). Nuclei are shown in green. Scale bar: 60 µm.
For quantification, the area of SA β-galactosidase staining was quantified and related to the number of cells. Data are means ± SEM of 3–5 independent experiments with three sections each. The mean number of SA β-galactosidase positivity in control incubations was set to 1 in each experiment. Data obtained after 48 or 72 h did not differ and were summarized in the graph. Statistics (ANOVA with Tukey multiple comparison test) were calculated separately for 0.01 and 0.001 µg samples. ***$p < 0.01$, compared to control cells.

occurred at concentrations larger than 500 µg/ml range. However, we cannot exclude subtle changes in gene expression which were not addressed in this study and may occur also at the low SPION concentrations used in our study (up to 5 µg/ml Fe). These were calculated as total iron concentration and were selected to match the iron concentration of MTO-loaded SPIONs, at which significant effects on cell behavior were observed.

During the application of drug-loaded SPIONs in magnetic drug targeting of solid tumors, most of the administered SPIONs are taken up by the target structure, but low concentrations remain in the circulation and are distributed to the organs. Therefore, in our studies, we used nanomolar rather than micromolar concentrations to evaluate the effects of MTO. Although, similar to control SPIONs, MTO-loaded SPIONs were primarily internalized by proximal cells, the biological effects of MTO were observed in both, proximal and distal cells due to the release of MTO from lauric acid-coated SPIONs upon exposure to the protein-containing epithelial cell specific medium.

MTO was introduced as anticancer drug in the 1980s and has been studied intensively since then. It is rapidly distributed from the blood into tissues resulting in a very high apparent volume of distribution (Ehninger et al., 1990; Hu et al., 1992; Scott & Figgitt, 2004). The drug is rapidly taken up by cells where it

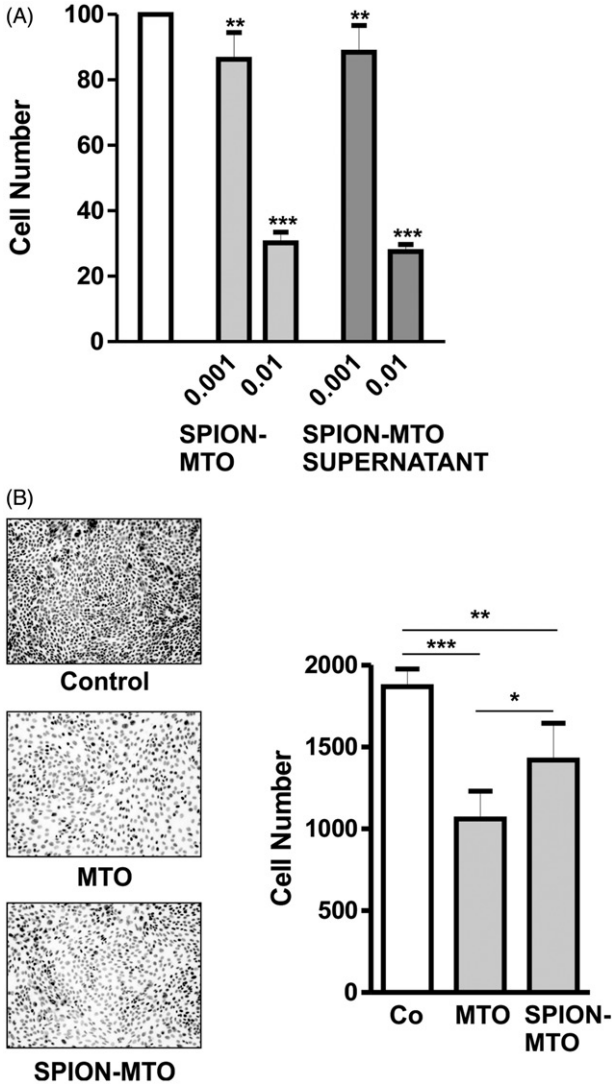

Figure 7. MTO is released from SPIONs into the epithelial cell culture medium.
(A) hTEC were incubated with SPION-MTO or with supernatants of centrifuged SPION-MTO. Cell numbers were determined after 72 h. Data are means ± SD four different experiments incubated with two different preparations of SPION-MTO. $^{**}p < 0.01$, $^{***}p > 0.001$, ANOVA with Tukey multiple comparison test.
(B) hTEC were seeded in transwell inserts and after reaching confluency were incubated with MTO or SPION-MTO (0.01 μg/ml) for 72 h. Nuclei were stained with DAPI. In each well, five images were randomly selected and cell numbers determined (means ± SD). $^{*}p<0.05$, $^{**}p < 0.01$, $^{***}p < 0.001$, ANOVA with Tukey multiple comparison test.

partitions into intracellular structures, membranes and cytoskeletal structures, binds to proteins and also DNA (Homolya et al., 2011). At micromolar concentrations of MTO, self-aggregation of the drug was observed *in vitro*, which may contribute to the long lasting accumulation of intracellular MTO (Feofanov et al., 1997). Nevertheless, MTO is relatively well tolerated in patients and renal injury does not play a major role as adverse effect in tumor therapy, or the more recently introduced treatment of multiple sclerosis with MTO (Cocco & Marrosu, 2014). This may be due to the fact that renal clearance only accounts for about 10% of the total MTO clearance in humans (Alberts et al., 1985; An & Morris, 2012; Savaraj et al., 1982). For this reason, data related to the effects of MTO on the cell biology of human tubular epithelial cells were not available. Regarding the dosage selected for our *in vitro* studies, the above-mentioned clearance data indicate that a standard dose of 12 mg/m^2 would result in an estimated urinary concentration of less than 500 ng/ml during the first 24 h, and significantly drop thereafter. The concentrations used in this study thus approximated concentrations which may also occur during treatment.

MTO belongs to the chemotherapeutic drugs which inhibit topoisomerase II and thus induce DNA strand breaks. Accumulation of DNA breaks may finally lead to cell death (McClendon & Osheroff, 2007). One of the early markers of DNA strand breaks is the phosphorylation of histone H2AX (Zhao et al., 2012). The phosphorylated form of histone H2AX (γH2AX) accumulates at DNA strand breaks and thus allows detection of intranuclear foci by immunocytochemistry (Rogakou et al., 1998). In our studies, some foci were positive for γH2AX even in control cells. This may reflect some DNA damage occurring during cell culture, but may also represent cells in M phase: The phosphorylation of histone H2AX in the absence of DNA strand breaks has previously been described in several proliferating human cell lines in M phase (Ichijima et al., 2005, McManus & Hendzel, 2005). Upon short term treatment with SPION-MTO at concentrations corresponding to nanomolar concentrations of MTO, a dose-dependent increase in γH2AX foci was observed in tubular epithelial cells. Prolonged incubation with MTO at nanomolar concentrations led to an inhibition of hTEC proliferation, but no overt necrosis or apoptosis were detected. Cells did not lose cell-cell contacts, but were flattened with enlarged cell bodies and an apparent increase in nuclear area. This phenotype was characteristic of senescence being induced by MTO-mediated inhibition of topoisomerase II in tumor cells (Zhao et al., 2010). Senescence was detected when tubular epithelial cells were cultured for 72 days starting with subconfluent cells, but was rarely observed in polarized cells where cell proliferation was inhibited, in line with previous data obtained in tumor cells (Zhao et al., 2010,2012). Nonproliferating tubular cells *in vivo* may thus be protected from induction of senescence by low concentrations of MTO.

MTO has also been reported to affect cellular functions independently of topoisomerase II inhibition. For example, treatment with MTO was shown to dose-dependently inhibit hypoxia inducible factor HIF-1α expression in a renal carcinoma cell line 769-P (Toh & Li, 2011). However, concentrations of MTO tested in that study were 10-fold higher than those used in our work. In our study, neither free MTO nor SPION-MTO modulated the expression of HIF-1α induced by pharmacological inhibition of prolyl hydroxylases (data not shown). In a porcine aortic endothelial line, MTO in the micromolar concentration range has furthermore been shown to affect F-actin structures by inhibition of Rho GTPases (Bidaud-Meynard et al., 2013). In earlier studies, we investigated inhibitors of Rho GTPases in primary tubular epithelial cells (Keller et al., 2012). However, we did not observe any changes in *F*-actin structures upon treatment of the hTEC cells with MTO, which was likely due to the much lower concentrations used in our studies as compared the study by Bidaud-Meynard et al (Bidaud-Meynard et al., 2013).

During the intraarterial application of the drug-loaded SPIONs for magnetic drug targeting of solid tumors, most of the administered SPIONs are taken up by the target structure, but low concentrations remain in the circulation and are distributed to the organs (Tietze et al., 2013). Therefore, in our studies, we used nanomolar rather than micromolar concentrations to evaluate the effects of MTO. Based on the results obtained with free MTO and control SPIONs, we expected selective effects of MTO-loaded SPIONs on proximal tubular epithelial cells. Although uptake of SPION-MTO was restricted to proximal cells during the first hours of incubation, the inhibition of topoisomerase II as visualized by γH2AX foci at DNA strand breaks was detectable both, in proximal and in distal cells. Moreover, inhibition of proliferation and induction of senescence were comparably

induced by free MTO and SPION-MTO, suggesting that MTO was released from SPIONs into the cell culture medium. These observations were in line with earlier studies which showed comparable effects of MTO and MTO-loaded SPIONS on T-lymphocytes (Janko et al., 2013). In the nanoparticle preparations used here, MTO was not covalently bound to the lauric acid-coated SPIONs, but use was made of its self-assembling adsorptive binding capacity (Janko et al., 2013; Tietze et al., 2013). Therefore, MTO may be released from SPIONs depending on the composition of the medium, especially if serum is present as in our experiments. This also relates to the *in vivo* situation, where over 95% of MTO in plasma is protein-bound (Hu et al., 1992). Additionally, MTO attached to SPIONs may be taken up by the cells upon cell-SPION contact and partition into cellular membranes, thus further contributing to MTO effects even in the distal tubular epithelial cells, in which SPION internalization is extremely low.

Conclusion

By utilizing primary human tubular epithelial cells with different endocytotic capacities, our model system allowed us to discriminate between the biological effects related to SPION uptake and those related to the released MTO. We show that whereas the uptake of SPIONs does not affect cellular functions or viability, the toxicity of drug-loaded SPIONs will depend essentially on the type of drug bound to nanoparticles. Considering the low systemic toxicity of MTO, the effects of SPION-MTO on hTECs were moderate, but they may become clinically relevant when more nephrotoxic drugs are bound to SPIONs.

Acknowledgements

The authors thank Eveline Schreiber for the preparation of SPIONs. Human kidney tissue was kindly provided by B. Wullich and his team, Department of Urology, FAU Erlangen. The authors are grateful to Jan Zaloga, Section of Experimental Oncology and Nanomedicine, for critical discussion of the manuscript.

Declaration of interest

The authors report no conflicts of interests related to this study. This study was supported by the DFG grant CI 162/2-1 and the Bavarian State Ministry of Environment and Consumer Protection.

Supplementary material available online.

References

Albanese A, Tang PS, Chan WC. 2012. The effect of nanoparticle size, shape, and surface chemistry on biological systems. Annu Rev Biomed Eng 14:1–16.

Alberts DS, Peng YM, Leigh S, Davis TP, Woodward DL. 1985. Disposition of mitoxantrone in cancer patients. Cancer Res 45: 1879–84.

Amstad E, Textor M, Reimhult E. 2011. Stabilization and functionalization of iron oxide nanoparticles for biomedical applications. Nanoscale 3:2819–43.

An G, Morris ME. 2012. A physiologically based pharmacokinetic model of mitoxantrone in mice and scale-up to humans: a semi-mechanistic model incorporating DNA and protein binding. Aaps J 14:352–64.

Bernd H, De Kerviler E, Gaillard S, Bonnemain B. 2009. Safety and tolerability of ultrasmall superparamagnetic iron oxide contrast agent: comprehensive analysis of a clinical development program. Invest Radiol 44:336–42.

Bidaud-Meynard A, Arma D, Taouji S, Laguerre M, Dessolin J, Rosenbaum J, et al. 2013. A novel small-molecule screening strategy identifies mitoxantrone as a RhoGTPase inhibitor. Biochem J 450: 55–62.

Cocco E, Marrosu MG. 2014. The current role of mitoxantrone in the treatment of multiple sclerosis. Expert Rev Neurother 14:607–16.

Dimri GP, Lee X, Basile G, Acosta M, Scott G, Roskelley C, et al. 1995. A biomarker that identifies senescent human cells in culture and in aging skin in vivo. Proc Natl Acad Sci USA 92:9363–7.

Ehninger G, Schuler U, Proksch B, Zeller KP, Blanz J. 1990. Pharmacokinetics and metabolism of mitoxantrone. A review. Clin Pharmacokinet 18:365–80.

Feofanov A, Sharonov S, Fleury F, Kudelina I, Nabiev I. 1997. Quantitative confocal spectral imaging analysis of mitoxantrone within living K562 cells: intracellular accumulation and distribution of monomers, aggregates, naphtoquinoxaline metabolite, and drug-target complexes. Biophys J 73:3328–36.

Gupta AK, Gupta M. 2005. Synthesis and surface engineering of iron oxide nanoparticles for biomedical applications. Biomaterials 26: 3995–4021.

Homolya L, Orban TI, Csanady L, Sarkadi B. 2011. Mitoxantrone is expelled by the ABCG2 multidrug transporter directly from the plasma membrane. Biochim Biophys Acta 1808:154–63.

Hu OY, Chang SP, Law CK, Jian JM, Chen KY. 1992. Pharmacokinetic and pharmacodynamic studies with mitoxantrone in the treatment of patients with nasopharyngeal carcinoma. Cancer 69:847–53.

Ichijima Y, Sakasai R, Okita N, Asahina K, Mizutani S, Teraoka H. 2005. Phosphorylation of histone H2AX at M phase in human cells without DNA damage response. Biochem Biophys Res Commun 336:807–12.

Janko C, Durr S, Munoz LE, Lyer S, Chaurio R, Tietze R, et al. 2013. Magnetic drug targeting reduces the chemotherapeutic burden on circulating leukocytes. Int J Mol Sci 14:7341–55.

Jeng HA, Swanson J. 2006. Toxicity of metal oxide nanoparticles in mammalian cells. J Environ Sci Health a Tox Hazard Subst Environ Eng 41:2699–11.

Keller C, Kroening S, Zuehlke J, Kunath F, Krueger B, Goppelt-Struebe M. 2012. Distinct mesenchymal alterations in N-cadherin and e-cadherin positive primary renal epithelial cells. PLoS One 7:e43584.

Kriz W, LeHir M. 2005. Pathways to nephron loss starting from glomerular diseases-insights from animal models. Kidney Int 67: 404–19.

Kroening S, Neubauer E, Wullich B, Aten J, Goppelt-Struebe M. 2010. Characterization of connective tissue growth factor expression in primary cultures of human tubular epithelial cells: modulation by hypoxia. Am J Physiol Renal Physiol 298:F796–806.

Laurent S, Saei AA, Behzadi S, Panahifar A, Mahmoudi M. 2014. Superparamagnetic iron oxide nanoparticles for delivery of therapeutic agents: opportunities and challenges. Expert Opin Drug Deliv 11: 1449–70.

Lyer S, Tietze R, Jurgons R, Struffert T, Engelhorn T, Schreiber E, et al. 2010. Visualisation of tumour regression after local chemotherapy with magnetic nanoparticles – a pilot study. Anticancer Res 30:1553–7.

McClendon AK, Osheroff N. 2007. DNA topoisomerase II, genotoxicity, and cancer. Mutat Res 623:83–97.

McManus KJ, Hendzel MJ. 2005. ATM-dependent DNA damage-independent mitotic phosphorylation of H2AX in normally growing mammalian cells. Mol Biol Cell 16:5013–25.

Nagai J, Takano M. 2014. Entry of aminoglycosides into renal tubular epithelial cells via endocytosis-dependent and endocytosis-independent pathways. Biochem Pharmacol 90:331–7.

Poettler M, Hofman S, Durr S, Wiest I, Zaloga J, Jeschke U, et al. 2014. Effect of BSA-coated superparamagnetic iron oxide nanoparticles on granulosa cells. Anticancer Res 34:6843–4.

Rogakou EP, Pilch DR, Orr AH, Ivanova VS, Bonner WM. 1998. DNA double-stranded breaks induce histone H2AX phosphorylation on serine 139. J Biol Chem 273:5858–68.

Saito A, Sato H, Iino N, Takeda T. 2010. Molecular mechanisms of receptor-mediated endocytosis in the renal proximal tubular epithelium. J Biomed Biotechnol 2010:403272.

Savaraj N, Lu K, Manuel V, Loo TL. 1982. Pharmacology of mitoxantrone in cancer patients. Cancer Chemother Pharmacol 8: 113–17.

Scott LJ, Figgitt DP. 2004. Mitoxantrone: a review of its use in multiple sclerosis. CNS Drugs 18:379–96.

Soenen SJ, Nuytten N, De Meyer SF, De Smedt SC, De Cuyper M. 2010. High intracellular iron oxide nanoparticle concentrations affect cellular cytoskeleton and focal adhesion kinase-mediated signaling. Small 6: 832–42.

Tietze R, Lyer S, Durr S, Struffert T, Engelhorn T, Schwarz M, et al. 2013. Efficient drug-delivery using magnetic nanoparticles-

biodistribution and therapeutic effects in tumour bearing rabbits. Nanomedicine 9:961–71.

Toh YM, Li TK. 2011. Mitoxantrone inhibits HIF-1α expression in a topoisomerase II-independent pathway. Clin Cancer Res 17:5026–37.

Wahajuddin Arora S. 2012. Superparamagnetic iron oxide nanoparticles: magnetic nanoplatforms as drug carriers. Int J Nanomedicine 7: 3445–71.

Winer JL, Liu CY, Apuzzo ML. 2012. The use of nanoparticles as contrast media in neuroimaging: a statement on toxicity. World Neurosurg 78:709–11.

Zaloga J, Janko C, Nowak J, Matuszak J, Knaup S, Eberbeck D, et al. 2014. Development of a lauric acid/albumin hybrid iron oxide nanoparticle system with improved biocompatibility. Int J Nanomedicine 9:4847–66.

Zhao H, Halicka HD, Traganos F, Jorgensen E, Darzynkiewicz Z. 2010. New biomarkers probing depth of cell senescence assessed by laser scanning cytometry. Cytometry a 77:999–1007.

Zhao H, Rybak P, Dobrucki J, Traganos F, Darzynkiewicz Z. 2012. Relationship of DNA damage signaling to DNA replication following treatment with DNA topoisomerase inhibitors camptothecin/topotecan, mitoxantrone, or etoposide. Cytometry a 81:45–51.

Zuehlke J, Ebenau A, Krueger B, Goppelt-Struebe M. 2012. Vectorial secretion of CTGF as a cell-type specific response to LPA and TGF-β in human tubular epithelial cells. Cell Commun Signal 10:doi:10.1186/1478-811X-10-25.

Supplementary materials available online.